



ELSEVIER

Comput. Methods Appl. Mech. Engrg. 191 (2002) 2483–2507

**Computer methods
in applied
mechanics and
engineering**

www.elsevier.com/locate/cma

Modeling delamination as a strong discontinuity with the material point method

H.L. Schreyer^{a,*}, D.L. Sulsky^b, S.-J. Zhou^c

^a *Department of Mechanical Engineering, University of New Mexico, 1105 Lawrence, NE Albuquerque, NM 87123, USA*

^b *Department of Mathematics and Statistics, University of New Mexico, Albuquerque, NM 87131, USA*

^c *Senior Product Engineer, GMATV—ITC 9900 Westpoint Drive, Suite 142, Indianapolis, IN 46033, USA*

Received 6 April 2001; received in revised form 26 September 2001; accepted 19 November 2001

Abstract

Decohesion is an important failure mode associated with layered composite materials. Here, the energy implications of material softening are explored in a thermodynamic framework with the result that the dissipated energy (fracture energy) is greater than the plastic work of the traction on the failure surface. It is also argued that if the traction and continuum constitutive equations are solved simultaneously, the resulting algorithm is as simple as that for conventional plasticity. For numerical simulations, the material point method displays the attributes of no mesh deformation so that remeshing is not necessary and the continuous tracking of material points avoids the need for remapping history variables such as decohesion. Compatibility is invoked in a weak sense with the result that no special algorithms are needed for mesh realignment along crack surfaces or for double nodes. Example solutions exhibit no sensitivity of delamination propagation with mesh orientation. © 2002 Published by Elsevier Science B.V.

Keywords: Material point method; Discontinuity; Material failure; Delamination

1. Introduction

As layered composite materials become stronger and more reliable, they are used in a broad range of applications that includes, for example, automobile parts and aircraft engine blades. With the increased potential for considerable loss of life if a segment should fail, there is a need for more comprehensive procedures to identify the location and the mode of failure. In addition to identifying the mode, it is also useful to determine if the failure is brittle, a process that could potentially have more catastrophic consequences than a ductile-type failure. Here, we focus on delamination, a type of failure that can occur in layered composites.

There are many criteria for material failure but the definitions of failure are often vague or defined implicitly through each criterion. We take material failure to mean the process by which two new free

* Corresponding author.

surfaces are formed, with brittle fracture as an obvious example. However, there are other forms of material failure as exemplified by ductile rupture [40], delamination, the breaking of grain boundaries and the pullout of reinforcing rods or fibers. Our interest is to represent approximately all of these phenomena with a single model that incorporates the essential features of the state of stress or strain at which failure initiates and that predicts the correct energy dissipated. Our focus is not on replicating the details of failure, although this can be done in some cases, but on predicting the effect of failure on the far-field stress distribution and on structural response as reflected, for example, by a force–deflection curve. The proposed approach is a constitutive equation that describes decohesion. When used with the material point method, which is a relatively new computational method that is particularly robust for problems with large deformations, the proposed approach has a simple structure in that the decohesion comes into the analysis through the constitutive equation only. There is no attempt to enforce the geometrical continuity of a crack. Instead, compatibility is enforced in an averaged sense.

Failure modeling involves both theoretical formulations of constitutive equations and numerical simulations, and the two aspects should be carefully delineated. However, the finite element method has become the method of choice for the majority of engineering applications so that the formulation of the constitutive equations is often tailored for use by finite elements; conversely limitations imposed by the finite element method are often interpreted unjustly as a limitation of the theoretical approach. In the following brief survey, we attempt to keep the discussion of the two phases distinct if at all possible.

A large number of papers related to failure have been based on a zone of softening with an assumed width in which a continuum constitutive equation continues to be used [5,10,11,18,23,32,44]. A theoretical difficulty with such an approach is the possible loss of ellipticity and material stability within the band. When used with finite elements, the band width is associated with the size of the elements and the accuracy is then limited when the elements become highly deformed.

An alternative (discrete) approach is to consider material failure as a strong discontinuity in displacement with traction related to the discontinuity. There is a long history in which discrete constitutive equations are postulated directly as reflected by Barenblatt [6], Hillerborg et al. [15], Needleman [22] and Planas et al. [28]. Feenstra et al. [13,14] and Corigliano [9] provide a nice summary of previous models and describe numerical methods based on the use of interface elements. The use of discrete constitutive equations has not met with complete favor partially because strong discontinuities are difficult to handle numerically and convergence with mesh refinement and mesh insensitivity is difficult to show although recent developments are very encouraging. The use of interface elements may require frequent remeshing if the crack surface propagates in a curved manner, and double nodes which separate with the evolution of decohesion [33]. The use of “constraint” elements is a related approach [31]. The work of Ortiz and coworkers [8,27,29] uses a combination of adaptive meshing with special cohesive elements to implement their constitutive model to obtain a robust formulation with correct propagation speeds and energy release. Dvorkin et al. [12] describe an alternative approach whereby discontinuities are handled at the element level rather than enforcing discontinuities to be along element boundaries. Wells and Sluys [41–43] have extended the concept with impressive results.

A fundamentally different approach for arriving at a description of failure is provided by Simo et al. [34] in which the continuum constitutive equation is extended beyond the loss of ellipticity condition into the softening regime. They argue that this extension should be accompanied by distribution theory which, in effect, leads to a strong discontinuity. The theory has since been extensively developed by Simo and Oliver [35], Armero and Garikipati [3], Larsson and Runesson [19], Oliver [24–26] and Armero [4]. The final result is also a discrete constitutive equation relating stress to the discontinuity in displacement, and here also the discontinuity is handled at the element or constitutive level.

We have opted for a particular combination of these ideas in an attempt to provide an approach that is as simple and as straightforward as possible. First, we propose the direct introduction of discrete constitutive equations with the thought that they should be introduced when ellipticity is lost, although a direct failure

initiation criterion can be used. No attempt is made to model the post-crack frictional effects that may occur with surfaces with rough cracks [13,14] although such features can be added. Second, the discontinuity is considered to be part of the constitutive equation and is applied in a manner analogous to that of Dvorkin et al. [12], Oliver [24,25] and Armero [4]. A point that is undergoing failure is also considered to be a material point in the continuum so that the decohesion and continuum constitutive equations must be simultaneously satisfied subject to the restriction of traction equilibrium. Third, we invoke the constitutive equation in the material point method. The arguments for the direct calculation of the strong discontinuity in displacement, which we also call decohesion, and the use of the material point method are summarized as follows:

(i) We retain the conceptual simplicity inherent with the discrete constitutive approach that material failure does not happen abruptly but occurs smoothly with a gradual reduction in traction as the displacement discontinuity increases.

(ii) We believe it is extremely difficult to evaluate properties of any constitutive equation in the failure regime. However, it is probably easier to select material parameters for a discrete constitutive equation than for a continuum model extended into the softening regime.

(iii) The discrete equation can be applied, if desired, at the instance ellipticity is lost so that there is a high probability that well posedness can be retained although a stability analysis must be performed [36].

(iv) The essential aspects of prescribed stress at the initiation of failure and prescribed energy dissipation at the end of failure are automatically included in this model, even for the case where the prescribed stress is not known, a priori, but follows from a bifurcation analysis.

(v) Once decohesion is initiated on a surface of discontinuity, the adjacent continuum tends to unload into the elastic regime, so the computational simplicity of only needing to combine decohesion with elasticity covers the vast majority of practical cases.

(vi) The decohesion constitutive equation can be developed in a thermodynamical setting, in concert with many current continuum models, and can include plasticity, damage, viscoelastic and viscoplastic features that are associated strictly with the decohesion.

(vii) The application of decohesion constitutive equations in the material point method retains the simplicity of current applications of strong discontinuities at the element level in the finite element method. However, double nodes or interface elements are not needed and there is the additional potential advantage that mesh orientation and mesh distortion are not factors that need to be considered.

(viii) Following the method outlined by Allix and Corigliano [2] there is the potential of relating the decohesion constitutive equation to mixed-mode fracture.

(ix) The use of a discrete constitutive equation may still be a suitable model for diffuse failure if the primary objective is to obtain an efficient solution for the region away from the failure zone.

(x) Finally, a discrete constitutive equation is a natural approach for modeling the failure of interfaces [16].

Section 2 provides only a brief description of the material point method since the method has been fully described in previous papers. Section 3 describes the basic structure of the decohesion model used in our analysis. Analytical and numerical solutions to model problems [45] including a convergence study are given in Section 4 which is then followed by conclusions concerning the general applicability of the method for material failure in general, including delamination.

2. The material point method

With the material point method [37–39] a solid body is discretized by marking a set of material points in the original configuration that are tracked throughout the deformation process. The deformation of the body satisfies Cauchy's equations of motion

$$\nabla \cdot \boldsymbol{\sigma} + \rho \mathbf{b} = \rho \mathbf{a} \quad (1)$$

in which ∇ denotes the gradient with respect to the current configuration, $\boldsymbol{\sigma}$ is the Cauchy stress, ρ the mass density, \mathbf{b} the specific body force and \mathbf{a} the acceleration. Transformations can be made as necessary to obtain alternative stress tensors for use in constitutive equations. Similarly, the appropriate strain tensor can be developed from the deformation gradient at the end of the previous load step and the velocity gradient at the current step with the assumption that the deformation with each step is infinitesimal. We are concerned here primarily with material failure of brittle materials so large rigid body motions may occur. However, since the strains are small, and our model problems preclude large rotations, we choose to focus the presentation on the essential aspects of the numerical simulation of decohesion in the context of small deformations.

Let \mathbf{x}_p^n , $p = 1, \dots, N_p$ denote the current position of material point p at time t^n , $n = 0, 1, 2, \dots$. These material points provide a Lagrangian description of the solid body that is not subject to mesh tangling. Each point at time t^n has an associated mass, m_p , density, ρ_p^n , velocity, \mathbf{v}_p^n , Cauchy stress tensor, $\boldsymbol{\sigma}_p^n$, strain, \mathbf{e}_p^n , and any other internal variables necessary for the constitutive model. If temperature changes are important, internal energy or temperature may also be ascribed to the material points. The material point mass is constant in time, insuring that the continuity equation is satisfied. Other variables must be updated with reference to conservation of momentum, conservation of energy, and a constitutive equation.

To make the computations tractable, at each time step of a dynamic algorithm information from the material points is interpolated to a background computational mesh. This mesh covers the computational domain and is chosen for computational convenience. A particularly simple choice is a regular rectangular grid. Of course, the background grid is not completely arbitrary since the part of the grid overlaying a body of material points must contain at least one material point per element for the algorithm to proceed. After information is interpolated to the grid, equations of motion are solved on this mesh which is considered to be an updated Lagrangian frame. For example, to solve the momentum equation on the grid using an explicit FE algorithm, one must know the value of the momentum at the beginning of the timestep at the nodal positions. The nodal momentum, $m_i^n \mathbf{v}_i^n$, is the product of the nodal mass and nodal velocity, and each is determined by interpolation,

$$\begin{aligned} m_i^n &= \sum_{p=1}^{N_p} m_p N_i(\mathbf{x}_p^n), \\ m_i^n \mathbf{v}_i^n &= \sum_{p=1}^{N_p} m_p \mathbf{v}_p^n N_i(\mathbf{x}_p^n). \end{aligned} \quad (2)$$

In the above, $N_i(\mathbf{x})$ is the nodal basis function associated with node i . In this paper, each function $N_i(\mathbf{x})$ is the tensor product of piecewise linear functions. The internal forces are determined from the particle stresses according to

$$\mathbf{f}_i^{\text{int}} = - \sum_{p=1}^{N_p} G_{ip}^n \boldsymbol{\sigma}_p^n m_p / \rho_p^n. \quad (3)$$

The quantity G_{ip}^n is the gradient of the nodal basis function evaluated at the material point position, $G_{ip}^n = \nabla N_i(\mathbf{x})|_{\mathbf{x}_p^n}$. The momentum equation is solved with the nodes considered to be moving with the deformation to give nodal velocities, \mathbf{v}_i^L , at the end of this Lagrangian time step of size Δt ,

$$m_i^n \frac{\mathbf{v}_i^L - \mathbf{v}_i^n}{\Delta t} = \mathbf{f}_i^{\text{int}}. \quad (4)$$

At the end of the Lagrangian step, the new nodal values of velocity are used to update the material points. The material points move along with the nodes according to the solution given throughout the elements by the nodal basis functions

$$\mathbf{x}_p^{n+1} = \mathbf{x}_p^n + \Delta t \sum_{i=1}^{N_n} \mathbf{v}_i^L N_i(\mathbf{x}_p^n). \quad (5)$$

Similarly, the material point velocity is updated via

$$\mathbf{v}_p^{n+1} = \mathbf{v}_p^n + \sum_{i=1}^{N_n} (\mathbf{v}_i^L - \mathbf{v}_i^n) N_i(\mathbf{x}_p^n). \quad (6)$$

The sums in these last two equations extend from 1 to N_n where N_n is the number of nodes in the computational mesh.

A strain increment for each material point is determined using the gradient of the nodal basis function,

$$\Delta \mathbf{e}_p = \frac{\Delta t}{2} \sum_{i=1}^{N_n} \left[G_{ip}^n \mathbf{v}_i^L + (G_{ip}^n \mathbf{v}_i^L)^T \right]. \quad (7)$$

This strain increment is then used in an appropriate constitutive equation for the material being modeled to update the stress at the material point. Any internal variables necessary in the constitutive model can also be assigned to the material points and transported along with them. Once the material points have been completely updated, the computational mesh may be discarded and a new mesh defined, if desired, and then the next timestep is begun.

Although a background mesh is used, the material point method has many of the positive features normally associated with meshless methods in which the computational discretization is continuously adjusted as a body deforms. As mentioned by Belytschko et al. [7], these methods are uniquely attuned to problems of large deformation, and to the propagation of interfaces such as material failure including cracks. Specific approaches include moving least squares with multiple scales and kernel methods [20] which are identical once the requirement of consistency is imposed. Moving least squares is a particular example of partitions of unity [21]. However, a common feature of these methods in their current forms is their computational cost and routine use for a wide range of applications appears not to be feasible. Currently, the cost of explicit forms of the element free Galerkin approach exceeds that of low-order elements by a factor of 4–10. An alternative approach which is much less complex and appears promising for problems involving penetration and perforation is that of smooth particle hydrodynamics [17,30]. Unfortunately, this method is subject to instabilities under tensile states of stress and must be applied carefully, particularly to failure involving fragmentation. Conservative smoothing and kernel renormalization are often necessary to stabilize and improve the accuracy of the procedure. Computational work is also quadratic in the number of particles since forces are computed via pairwise interactions, although this can be alleviated using complicated data structures such as quadtrees and oct-trees.

In comparison with the above methods, the material point method appears to be considerably less complex with a cost increase for explicit time integration of about 20% over that associated with the use of low-order finite elements. The approach involving a combination of a background mesh and material points can accommodate large deformations without mesh tangling. Since the computational mesh is under user control, it can be chosen so that reasonable time steps may be taken in this Lagrangian frame. Usually, the time step is restricted by the CFL condition for an explicit algorithm, where the critical time step is the ratio of the mesh size to the wave speed. Note that this condition depends on the more favorable mesh spacing, not the material point spacing. Since equations are solved in an updated Lagrangian frame on the FE mesh, the nonlinear convective terms troublesome in Eulerian formulations are not an issue. Finally, since the material properties and internal variables are assigned to the material points, the values of these parameters do not change as the material points are transported to new locations.

3. Discrete constitutive equation for decohesion

3.1. The theoretical model

We define the initiation of material failure as the time when a material point first experiences a discontinuity in displacement but continues to function as a point in a solid continuum. A collection of such points in a neighborhood defines a failure surface, Γ . Although the material manifestation is a single surface, one observes spatially two surfaces, Γ_1 and Γ_2 , as sketched in Fig. 1. Each dotted line illustrates points in space identified with a single material point which can be considered associated with any one of the spatial points on the line. The sketch illustrates the material surface as a thick line between the two spatial surfaces but if a Lagrangian description is used, the material surface may be at a totally different location. Failure is said to be complete when traction can no longer be sustained on the material surface, i.e., the spatial surfaces no longer have any ligaments connecting them even though one point on each surface is identified as a single material point. This discontinuity in displacement is called decohesion.

Here, we present a development of discrete constitutive equations using thermodynamics as a framework with the result that the dissipation inequality is automatically satisfied. The approach entails two essential assumptions consisting of (i) the form of the free energy, and (ii) the form of the evolution equations. Each assumption leads to a different model which can only be tested by solving a problem for which either qualitative or quantitative data exist. To allow for the presentation of different models in a convenient manner, we present the general framework first, and then show the implications inherent in specific assumptions.

The formulation of the discrete constitutive equation is analogous to what one might use for a rigid-plastic continuum for which the elastic part of the response is ignored, i.e., the total strain and the plastic strain are identical. Then the elastic internal strain energy does not exist and the stress must be provided by the solution to a boundary value problem. However, there remains a contribution to the free energy associated with hardening and evolution equations for plasticity variables.

Consider a situation where loads are applied to a body that is continuous except on a material failure surface, Γ , which displays a strong discontinuity, or decohesion, $\mathbf{u}^d = [\mathbf{u}]$. Any point on the surface is also a point in the continuum which is assumed to be governed by linear elasticity so that the stress, $\boldsymbol{\sigma}$, and strain, \mathbf{e} , are linearly related by the elasticity tensor, \mathbf{E} :

$$\boldsymbol{\sigma} = \mathbf{E} : \mathbf{e}. \tag{8}$$

If \mathbf{n} denotes the normal to the surface, then the traction, $\boldsymbol{\tau}$, is given by $\boldsymbol{\tau} = \boldsymbol{\sigma} \cdot \mathbf{n}$. The rate at which power is being added to the surface by this traction is $\boldsymbol{\tau} \cdot \dot{\mathbf{u}}^d$ in which a superposed dot denotes a derivative with respect to time. We postulate that the free energy per unit surface area consists of an initial energy, U_0 , due to residual stresses that could result from a curing process, and a term, U_d , which represents the effect of decohesion:

$$U = U_0 - U_d(\bar{\mathbf{u}}). \tag{9}$$

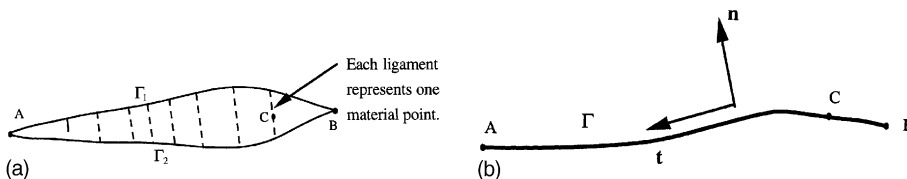


Fig. 1. Material failure as represented by two spatial surfaces, Γ_1 and Γ_2 , or one material surface, Γ : (a) decohesion in the spatial configuration: two surfaces, (b) decohesion in the material configuration: surface with discontinuity.

The use of the negative sign is meant to suggest that normally energy is provided by the original material to the decohesion process. The parameter, \bar{u} , is a scalar representation of the state of decohesion. A specific choice for U_d (positive) provides part of the decohesion constitutive model. The decohesion, \mathbf{u}^p , is viewed as “permanent” decohesion and is introduced similarly to plastic strain in elasto-plastic continuum models. In the absence of elasticity, $\mathbf{u}^p = \mathbf{u}^d$.

If only \mathbf{u}^p and \bar{u} are considered to be the primary variables describing decohesion, the dissipation power is

$$D_s = \boldsymbol{\tau} \cdot \dot{\mathbf{u}}^d - \dot{U} = \boldsymbol{\tau} \cdot \dot{\mathbf{u}}^p + \bar{\boldsymbol{\tau}} \dot{\bar{u}} \quad \text{with } \bar{\boldsymbol{\tau}} = \frac{\partial U_d}{\partial \bar{u}}. \tag{10}$$

The generalized traction, $\bar{\boldsymbol{\tau}}$, is conjugate to \bar{u} . Instead of the traction starting at zero, as it does for some existing discrete models [9,22], we visualize that when the failure process starts, $\mathbf{u}^d = \mathbf{0}$, $\mathbf{u}^p = \mathbf{0}$, and the traction is the initial vector, $\boldsymbol{\tau}_0$, which depends on the history of the stress path.

We parameterize the development of decohesion through a single, dimensionless monotonically increasing variable, λ , and the evolution equations

$$\dot{\mathbf{u}}^p = \dot{\lambda} \mathbf{m}^e, \quad \dot{\bar{u}} = \dot{\lambda} m^e \tag{11}$$

in which \mathbf{m}^e and m^e denote evolution functions that depend on $\boldsymbol{\tau}$ and $\bar{\boldsymbol{\tau}}$. \mathbf{m}^e is a vector whose inner product with $\boldsymbol{\tau}$ is assumed to be positive, semi-definite. If we introduce an effective traction

$$\boldsymbol{\tau}^e = \boldsymbol{\tau} \cdot \mathbf{m}^e, \tag{12}$$

then the dissipation power becomes

$$D_s = \dot{\lambda} [\boldsymbol{\tau}^e + \bar{\boldsymbol{\tau}} m^e]. \tag{13}$$

To ensure the dissipation power is positive, define a decohesion function as follows:

$$F_d = \boldsymbol{\tau}^e + \bar{\boldsymbol{\tau}} m^e - \tau_0^e, \quad \tau_0^e > 0. \tag{14}$$

The function has been constructed in the usual manner so that F_d is negative when the traction components are zero. We assume decohesion does not occur unless $F_d = 0$ in which case the dissipation power becomes $D_s = \dot{\lambda} \tau_0^e$, a positive scalar (and $F_d > 0$ is not permitted). The evolution equations can now be interpreted as parameterized in terms of dissipation power which is a monotonically increasing parameter. The total dissipated energy is simply $\lambda \tau_0^e$ which depends only on the value of λ and not on the path followed.

Next, we consider the decohesion condition, $F_d = 0$. At the initiation of decohesion, $\boldsymbol{\tau} = \boldsymbol{\tau}_0$ and $\mathbf{m}^e = \mathbf{m}_0^e$. If we assume $\bar{\boldsymbol{\tau}} = 0$ at the initiation, then

$$\tau_0^e = \boldsymbol{\tau}_0 \cdot \mathbf{m}_0^e. \tag{15}$$

Typically, $\bar{\boldsymbol{\tau}}$ increases until $\boldsymbol{\tau}^e = 0$, the point defined to be separation. The values of $\bar{\boldsymbol{\tau}}$, m^e , \mathbf{u}^p and \bar{u} at separation are denoted by $\bar{\boldsymbol{\tau}}_s$, m_s^e , \mathbf{u}_s^p and \bar{u}_s , respectively, where $\bar{\boldsymbol{\tau}}_s = \tau_0^e / m_s^e$. Unless there is a load reversal which brings the two spatial surfaces back into contact, it is assumed that $\boldsymbol{\tau}^e$ remains zero after separation.

With the use of (9), the stored surface energy lost due to separation is

$$\Phi_U = -U_d(\bar{u}_s). \tag{16}$$

The total energy per unit area that must be provided to cause total separation is variously called the fracture energy, or the energy of separation, Φ_F , and consists of the sum of the stored energy and the dissipated energy:

$$\Phi_F = \Phi_U + \Phi_D. \tag{17}$$

Because Φ_U is negative, the fracture energy is less than the dissipation.

In summary, the resulting set of constitutive equations becomes

(i) $\dot{\boldsymbol{\sigma}} = \mathbf{E} : \dot{\boldsymbol{\epsilon}}$	Continuum elasticity	
(ii) $\dot{\mathbf{t}} = \dot{\boldsymbol{\sigma}} \cdot \mathbf{n}$	Traction equilibrium	
(iii) $\dot{\mathbf{u}}^p = \dot{\lambda} \mathbf{m}^e, \quad \dot{\bar{u}} = \dot{\lambda} m^e$	Evolution equations	(18)
(iv) $\bar{\tau} = \partial U_d / \partial \bar{u}$	Constitutive equation	
(v) $F_d \equiv \tau^e - (\tau_0^e - \bar{\tau} m^e) = 0$	Consistency	
(vi) $\tau^e = \boldsymbol{\tau} \cdot \mathbf{m}^e$ and $\tau_0^e = \boldsymbol{\tau}_0 \cdot \mathbf{m}_0^e$	Definition of internal variables	

Two additional assumptions remain to completely formulate constitutive equations: (i) the form of the evolution functions \mathbf{m}^e and m^e , and (ii) the form of the function U_d which provides a constitutive relation between $\bar{\tau}$ and \bar{u} . Even slight changes in the forms of these functions can have significant effects on predictions. Since the only possible way to evaluate the suitability of decohesive constitutive equations is indirectly through comparisons of solutions to problems with features provided by experimental data, we consider (18) to be the basic format and provide different models based on plausible assumptions. The results of choosing specific forms for \mathbf{m}^e , m^e and U_d are given next.

3.1.1. Model 1: associated evolution equations

Here we are more specific in our formulation of the decohesion model. In the theoretical formulation, it is most convenient to use dimensional parameters so that physical interpretations can be easily made; conversely, for numerical implementation of the theory, dimensionless variables should be used. With this objective in mind, we choose λ to be dimensionless and consider \bar{u} to have the dimension of length (in analogy with the decohesion \mathbf{u}^d). We choose the evolution functions and the decohesion energy to be of the following forms:

$$\mathbf{m}^e = \bar{u}_0 \frac{\mathbf{A}_d \cdot \boldsymbol{\tau}}{(\boldsymbol{\tau} \cdot \mathbf{A}_d \cdot \boldsymbol{\tau})^{1/2}}, \quad m^e = \bar{u}_0, \quad U_d = U_0 \frac{(\bar{u}/\bar{u}_0)^{q+1}}{(q+1)} \quad (19)$$

in which \mathbf{A}_d is taken to be a positive definite (dimensionless) tensor whose components are material parameters, as is $q \geq 0$. Additional material parameters (constants) are the reference decohesion scalar, \bar{u}_0 , and the reference surface energy, U_0 . We define a reference scalar traction, $\bar{\tau}_0$, by the relation $U_0 = \bar{u}_0 \bar{\tau}_0$. The immediate result of these choices is that

$$\tau^e = \bar{u}_0 (\boldsymbol{\tau} \cdot \mathbf{A}_d \cdot \boldsymbol{\tau})^{1/2}, \quad \bar{u} = \lambda \bar{u}_0, \quad \bar{\tau} = \bar{\tau}_0 (\lambda)^q \quad (20)$$

and the evolution functions are obtained as derivatives of the damage function with respect to the corresponding conjugate variables, i.e., the evolution functions are said to be “associated”:

$$\mathbf{m}^e = \frac{\partial F_d}{\partial \boldsymbol{\tau}}, \quad m^e = \frac{\partial F_d}{\partial \bar{\tau}}. \quad (21)$$

At this point we consider a two-dimensional formulation with \mathbf{n} denoting the normal to the failure surface and \mathbf{t} a unit tangent vector as indicated in Fig. 1. Corresponding components of $\boldsymbol{\tau}$ are τ_n and τ_t , respectively. If the traction consists only of a normal component, specify the failure initiation value as τ_{nf} and, similarly, let τ_{tf} denote the failure initiation value for a purely shear case. One approach for incorporating these failure initiation conditions is to choose the components of \mathbf{A}_d with respect to this local basis as follows:

$$[\mathbf{A}_d] = \bar{\tau}_0^2 \begin{bmatrix} 1/(\tau_{nf})^2 & 0 \\ 0 & 1/(\tau_{tf})^2 \end{bmatrix}. \quad (22)$$

The consequences of this choice are

$$\begin{aligned}
 D_s &= \dot{\lambda}U_0, \quad \bar{\tau}^* \equiv \frac{\bar{\tau}}{\bar{\tau}_0} = \lambda^q, \quad F_d = U_0F_d^*, \quad F_d^* = \tau^{e^*} - (1 - \bar{\tau}^*), \\
 \tau^e &= U_0\tau^{e^*}, \quad \tau^{e^*} = \frac{(\boldsymbol{\tau} \cdot \mathbf{A}_d \cdot \boldsymbol{\tau})^{1/2}}{\bar{\tau}_0} = \left(\frac{\tau_n^2}{\tau_{nf}^2} + \frac{\tau_t^2}{\tau_{tf}^2} \right)^{1/2}
 \end{aligned}
 \tag{23}$$

where τ^{e^*} is a dimensionless effective traction, $\bar{\tau}^*$ is a dimensionless form of $\bar{\tau}$, and F_d^* is a dimensionless decohesion function. The conditions at the initiation of decohesion are $\bar{u} = 0$ and $\tau^{e^*} = 1$ so that $\tau_0^e = U_0$, a condition used in (23).

We note that the decohesion condition ($F_d^* = 0$) reduces to $\tau^{e^*} = 1 - \bar{\tau}^*$. As decohesion occurs \bar{u} increases and τ^{e^*} decreases to zero when $\bar{u} = \bar{u}_0$. Therefore \bar{u}_0 can be interpreted as the value of \bar{u} at which separation occurs. In the post separation regime, $\bar{u} > \bar{u}_0$, the decohesion condition is $\tau^{e^*} = 0$. Finally, we give an alternative form for the decohesion evolution function:

$$\mathbf{m}^e = \frac{U_0}{\tau^{e^*}} \left(\frac{\tau_n}{\tau_{nf}^2} \mathbf{n} + \frac{\tau_t}{\tau_{tf}^2} \mathbf{t} \right).
 \tag{24}$$

Since the dissipation rate is $\dot{\lambda}U_0$, the energy dissipated per unit surface area at any moment is simply λU_0 . From (20), $\lambda = 1$ at separation so the maximum energy dissipated is U_0 which provides a physical interpretation and a method for determining this particular parameter. The formulation implies the dissipated energy is independent of path which is generally not representative of real materials. The final value of the stored energy is obtained by substituting $\bar{u} = \bar{u}_0$ in (19) and using (16). In summary, the final dissipated, stored and total failure energies are

$$\Phi_D = U_0, \quad \Phi_U = -\frac{1}{(q+1)}U_0, \quad \Phi_F = \frac{q}{(q+1)}U_0.
 \tag{25}$$

For the given model, the required data are τ_{nf} , τ_{tf} , U_0 and q . We can choose $\bar{\tau}_0 = \tau_{nf}$ and then $\bar{u}_0 = U_0/\bar{\tau}_0$ to provide values for all of the parameters. Suppose a pure opening-mode path is followed, or $\tau_t = 0$. Then it is easily shown that the normal component of the decohesion is $u_n^p = \bar{u}(\bar{\tau}_0/\tau_{nf})$. If $\bar{\tau}_0$ is chosen to equal τ_{nf} , then \bar{u} equals u_n^p for Mode I. Experimental data obtained from a pure shear mode test can then be used to assess the adequacy of the model in a process similar to that used to evaluate a Mises plasticity model whose parameters are selected using data from a uniaxial stress test.

Sometimes non-associated models are required to provide a better fit with experimental data including observations on the mode of failure. Next we give an example of how a particular non-associated model can be constructed.

3.1.2. Model 2: non-associated evolution functions

Suppose we retain all aspects of the previous model with the exception that the evolution equation for the permanent decohesion is in the normal, or opening, direction irrespective of the state of traction:

$$\dot{u}_n^p = \dot{\lambda}m_n^e, \quad \dot{u}_t^p = 0, \quad m_n^e = \mathbf{m}^e \cdot \mathbf{n}.
 \tag{26}$$

We retain the previous expression for τ^e and the decohesion function. Therefore, the dissipation rate for normal mode decohesion must be evaluated specifically from the following equation:

$$D_{s,n} = \boldsymbol{\tau} \cdot \dot{\mathbf{u}}^p + \bar{\tau} \dot{\bar{u}} = \dot{\lambda}[\tau_n u_n^p + \bar{\tau} \bar{u}_0]
 \tag{27}$$

which will be less than that obtained with the associated rule (sometimes called the principle of maximum dissipation) if τ_t is not zero for at least part of the decohesion. A corresponding development for Mode II (pure shear) evolution can be obtained by merely replacing normal components of traction with shear components.

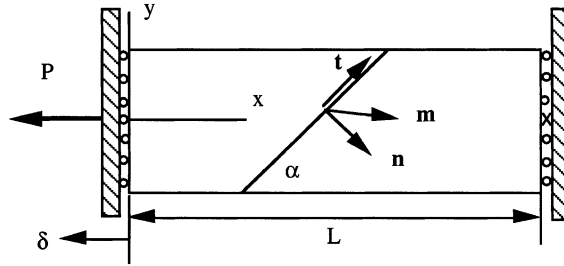


Fig. 2. Notation and parameters associated with the model problem.

3.2. Solution to a model problem

We take as the basic model problem the case of a bar of length L , height h and unit depth, with the center point at one end fixed, the other end extended, and both ends are constrained against rotation as indicated in Fig. 2. The extension is denoted by δ and the resultant force is P . The problem is considered to be one of plane stress in the x - y plane. The bar is composed of a uniform laminated material with the laminates forming an angle of α with respect to the x - z plane. The only failure mode considered is that of delamination. Therefore, all failure planes are identified by the fixed unit normal, \mathbf{n} . The unit tangent vector, \mathbf{t} , is included in the figure for the sake of completeness. Typically failure initiates at a weak point on one laminate surface and propagates across the bar so the problem is actually two-dimensional and can only be solved numerically. However, approximate solutions can be obtained analytically if the following assumptions are made: (i) the stress is uniaxial everywhere, and (ii) decohesion occurs uniformly across the bar. Solutions based on these assumptions provide an indication of the features of the solution for a wide range of problem parameters and serve to validate the numerical procedure.

With the assumption of uniaxial stress in a bar of unit depth and width H , the only non-zero stress component is $\sigma_{xx} = \sigma = P/H$. The geometry of the problem provides the following relations:

$$\begin{aligned} \mathbf{n} &= \sin \alpha \mathbf{e}_x - \cos \alpha \mathbf{e}_y, & \mathbf{t} &= \cos \alpha \mathbf{e}_x + \sin \alpha \mathbf{e}_y, \\ \tau_n &= \sigma \sin^2 \alpha, & \tau_t &= \sigma \sin \alpha \cos \alpha. \end{aligned} \quad (28)$$

If we define the constant scalar, σ_0 , and the constant vector, \mathbf{m}_c^e , by

$$\frac{1}{\sigma_0} = \sin \alpha \left[\frac{\sin^2 \alpha}{\tau_{nf}^2} + \frac{\cos^2 \alpha}{\tau_{tf}^2} \right]^{1/2}, \quad \mathbf{m}_c^e = U_0 \sigma_0 \sin \alpha \left(\frac{\sin \alpha}{\tau_{nf}^2} \mathbf{n} + \frac{\cos \alpha}{\tau_{tf}^2} \mathbf{t} \right), \quad (29)$$

then

$$\mathbf{A}_d \cdot \boldsymbol{\tau} = \frac{\bar{\tau}_0}{\bar{\mathbf{u}}_0} \frac{\sigma}{\sigma_0} \mathbf{m}_c^e, \quad \tau^c = U_0 \frac{\sigma}{\sigma_0} \quad \text{and} \quad \mathbf{m}^c = \mathbf{m}_c^e \quad (30)$$

with the assumption of an associated flow rule. The bar is loaded elastically until the stress reaches the value σ_0 at which point decohesion is first indicated ($\tau^c = U_0$). From this point on, with the assumption that the loading continually induces decohesion, the consistency condition implies that

$$\sigma = \sigma_0 (1 - \lambda^q) \quad \text{or} \quad \lambda = \left(1 - \frac{\sigma}{\sigma_0} \right)^{1/q} \quad (31)$$

with separation occurring when $\lambda = 1$. The evolution equation for the permanent decohesion (total decohesion) reduces to $\dot{\mathbf{u}}^p = \dot{\lambda} \mathbf{m}_c^e$ which can be integrated to obtain $\mathbf{u}^p = \lambda \mathbf{m}_c^e$. Therefore, with the use of (31) and (29), we obtain the components

$$u_x^p = \left(1 - \frac{\sigma}{\sigma_0}\right)^{1/q} U_0 \frac{1}{\sigma_0 \sin \alpha}, \quad u_y^p = \left(1 - \frac{\sigma}{\sigma_0}\right)^{1/q} U_0 \sigma_0 \sin^2 \alpha \cos \alpha \left(\frac{1}{\tau_{tf}^2} - \frac{1}{\tau_{nf}^2}\right). \tag{32}$$

If E is Young’s modulus, the bar experiences a homogeneous strain $e = \sigma/E$ for loading from zero stress up to the point $\sigma = \sigma_0$. After decohesion begins, the elongation of the bar, δ , must include the discontinuity, or

$$\delta = eL + u_x^p. \tag{33}$$

For this second phase involving decohesion and a decrease in stress (post-peak regime), the average strain, $e_{ave} = \delta/L$, is

$$e_{ave} = \frac{\sigma_0}{E} [\sigma^* + (1 - \sigma^*)^{1/q} \eta], \quad \sigma^* = \frac{\sigma}{\sigma_0} \tag{34}$$

in which the key dimensionless parameter, η , is defined by a product of dimensionless parameters:

$$\eta = \frac{1}{\sin \alpha} \left(\frac{\bar{u}_0}{L}\right) \left(\frac{\bar{\tau}_0}{\sigma_0}\right) \left(\frac{E}{\sigma_0}\right). \tag{35}$$

To illustrate the effects of dimensionless parameters on the response of a bar, it is conventional to display the result as force versus deflection. The peak force is simply $P_{max} = \sigma_0 H$. The slopes in the elastic and softening regimes become

$$\left. \frac{dP}{d\delta} \right|_{elas} = \frac{EH}{L}, \quad \left. \frac{dP}{d\delta} \right|_{soft} = \frac{EH}{L} \frac{1}{(1 - (\eta/\hat{P}))} \quad \text{with } \hat{P} \equiv q \left(1 - \frac{P}{P_{max}}\right)^{(1/q)-1}. \tag{36}$$

Normally, the post-peak behavior consists of a monotonic decrease of load with displacement so that $dP/d\delta$ is negative. However, if η is sufficiently small the slope may be positive and this feature indicates a load reversal that is sometimes called snapback. For the special case of $q = 1$, load reversal occurs if $\eta < 1$. It follows from (35) that it is always possible to obtain load reversal by simply taking a long enough specimen. The angle of the failure also plays a significant role. Recall from (29) that the strengths in the normal mode and shear mode, and α , appear in the expression for σ_0 .

When $q \neq 1$, the slope varies with the stress but values of η can still be selected which will display load reversal. If load reversal can exist, the interpretation of experimental data must be performed with care because, with a displacement prescribed loading device, snap down will occur and an incorrect measure of energy absorption will be obtained. With regard to numerical simulations, special algorithms must be constructed to provide solutions with load reversal.

Typical response curves based on (34) for various values of q and η are shown in Fig. 3 to illustrate the general features that are reflected by the decohesion constitutive equation as applied to the axial loading of a bar. Fig. 3(i), (ii) and (iii) correspond to values of $q = 0.8, 1.0$ and 1.2 , respectively, with the inserts showing the respective softening functions. The curves labeled a, b and c correspond to values of $\eta = 0.75, 1.25$ and 2.0 respectively.

If the decohesion is constrained to be only an opening mode, then

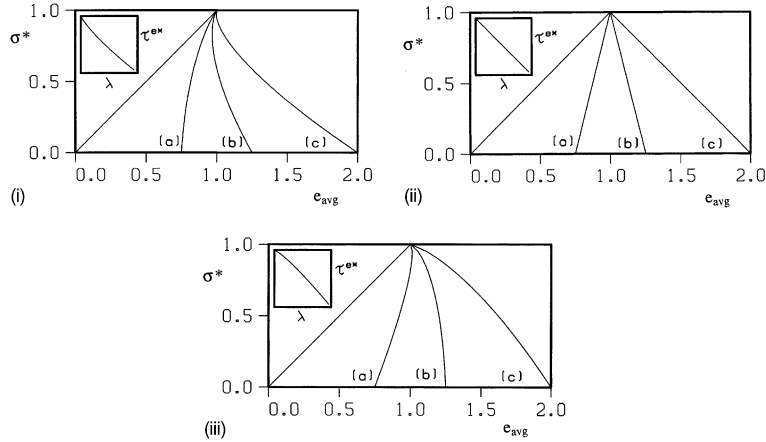


Fig. 3. Dimensionless stress, $\sigma^* = P/P_{\max}$, versus average strain, e_{avg} , for decohesion of a bar for various values of q and η : (a) $\eta = 0.75$, (b) $\eta = 1.25$, (c) $\eta = 2.0$. (i) $q = 0.8$, (ii) $q = 1.0$, (iii) $q = 1.2$.

$$\begin{aligned}
 m_n^c &= U_0 \frac{\sigma_0 \sin^2 \alpha}{\tau_{\text{nf}}^2}, \\
 u_x^p &= U_0 (1 - \sigma^*)^{1/q} \frac{\sigma_0 \sin^3 \alpha}{\tau_{\text{nf}}^2}, \\
 u_y^p &= -U_0 (1 - \sigma^*)^{1/q} \frac{\sigma_0 \sin^2 \alpha \cos \alpha}{\tau_{\text{nf}}^2},
 \end{aligned}
 \tag{37}$$

and load deflection curves analogous to those in Fig. 3 can be obtained. A similar situation holds if the mode is constrained to be one of pure shear.

3.3. Summary comments

Here we summarize the results of this section. The framework for a class of decohesion models consistent with thermodynamical concepts has been provided. The essential ideas are:

- (i) The decohesion constitutive equation is applied simultaneously with the continuum constitutive equation (elasticity is given here but any other constitutive equation can be used).
- (ii) As softening occurs, the sum of the work performed by the traction and the stored energy released by the material equals the energy dissipated.
- (iii) The example decohesion constitutive equation included in (18), (19) and (22) includes four material parameters which consist of U_0 , the dissipated energy per unit failure surface (fracture energy), the maximum sustainable values of traction, τ_{nf} , under pure Mode I and τ_{tf} , under pure Mode II, and a parameter q which provides a non-linear aspect to the softening function.
- (iv) The material parameters, U_0 , τ_{nf} and τ_{tf} can often be assigned directly from experimental data available in the literature. A value for the parameter, q , can be determined indirectly by fitting theoretical predictions to experimental data on a structural element such as the tensile failure of a uniaxial stress specimen.

4. Numerical applications

A bar subject to failure due to delamination does not exhibit uniaxial stress in the vicinity of the initiation of decohesion. In fact the stress path is quite complex and can only be reflected by a detailed analysis involving the assumption of plane stress for a bar that is thin with respect to its height. Nevertheless, the overall response should be close to that obtained under the assumption of uniaxial stress so that the solutions of the previous section can serve as part of the verification of a numerical method. The modeling of the propagation of a discontinuity at an arbitrary angle through a mesh may introduce significant but not quantifiable numerical errors. Here, we show that the material point method provides the basis for a simple algorithm with numerical results in agreement with the one-dimensional solutions for propagation of delamination at any angle across the mesh.

4.1. Incorporation with the material point method

In general, there is no need to determine the actual shape of the deformed material element associated with each material point. However, when material separation occurs, there is a need to consider the effect on the strain field over the element (compatibility). To illustrate the process, we consider small deformations so that the original configuration can be used. However, decohesion, and especially separation, represent large deformations. Typically, each cell with the material point method is chosen to be a square element with each side of length h . Over each element, the increment in strain, $\Delta \mathbf{e}$, and the increment in decohesion, $\Delta \mathbf{u}^d$, are approximated by constants as indicated in Fig. 4 which also shows the unit vector $\mathbf{m} = \Delta \mathbf{u}^d / |\Delta \mathbf{u}^d|$. For future use, define the opening, \mathbf{M}_n , shear, \mathbf{M}_t , and failure, \mathbf{M}_m , tensor modes as follows:

$$\mathbf{M}_n = \mathbf{n} \otimes \mathbf{n}, \quad \mathbf{M}_t = \frac{1}{2}(\mathbf{n} \otimes \mathbf{t} + \mathbf{t} \otimes \mathbf{n}), \quad \mathbf{M}_m = \frac{1}{2}(\mathbf{n} \otimes \mathbf{m} + \mathbf{m} \otimes \mathbf{n}). \quad (38)$$

We note that \mathbf{M}_m reduces to \mathbf{M}_n and \mathbf{M}_t when $\mathbf{m} = \mathbf{n}$ and $\mathbf{m} = \mathbf{t}$, respectively.

For a given time increment, if the total (average) strain increment, $\Delta \mathbf{e}$, is considered fixed, the result of the decohesion is that the effective strain increment in the remaining part of the material in the element must be reduced (relaxed) by what might be called a decohesion strain increment, $\Delta \mathbf{e}^d$, which satisfies a weak form of the compatibility condition

$$\int_{\Omega_e} \Delta \mathbf{e}^d dV = \int_{\partial \Omega_d} \Delta u^d \mathbf{M}_m dA, \quad \Delta \mathbf{u}^d = \Delta u^d \mathbf{m} \quad (39)$$

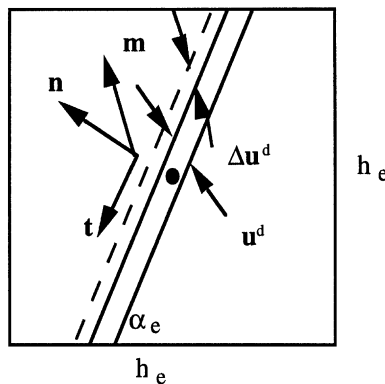


Fig. 4. A typical element with decohesion.

in which dV and dA denote differentials of volume on the element, Ω_e , and of area on the decohesion surface, $\partial\Omega_d$, respectively. The magnitude of the decohesion increment, which is in the direction of \mathbf{m} by definition, is Δu^d . With the assumptions that the decohesion and strain are constant over each element, the result is the following expression relating the “relaxation” or “decohesion” strain increment to the increment in decohesion:

$$\Delta \mathbf{e}^d = \frac{\Delta u^d}{L_e} \mathbf{M}_m, \quad L_e = \frac{V_e}{A_d}. \quad (40)$$

The effective length, L_e , is merely the ratio of the element volume to the area of the decohesion surface within that element. For the two-dimensional case illustrated in Fig. 4, the effective length is

$$L_e = h_e \sin \alpha_e, \quad \pi/4 \leq \alpha_e \leq \pi/2 \quad (41)$$

with a corresponding formula for an angle measured with respect to the vertical side of the material element if $\alpha_e < \pi/4$.

4.2. Solution algorithm

The constitutive equations subroutine is invoked with the total strain increment, $\Delta \mathbf{e}$, prescribed, with the total decohesion equal to the plastic decohesion, and with \mathbf{n} given and assumed fixed. It is computationally more efficient to define an alternative mode vector, \mathbf{m}^* , from which the mode vector, \mathbf{m}^e , and an alternative tensor mode, \mathbf{M}^* , are easily determined. Let $\boldsymbol{\sigma}_{pr}$, \mathbf{u}_{pr}^p and λ_{pr} denote the values of $\boldsymbol{\sigma}$, \mathbf{u}^p and λ , respectively, at the end of the previous step. The requirement is to solve the following set of non-linear equations:

$$\begin{aligned} \Delta \boldsymbol{\sigma} &= \Delta \boldsymbol{\sigma}^{tr} - \mathbf{E} : \Delta \mathbf{e}^d, & \Delta \boldsymbol{\sigma}^{tr} &= \mathbf{E} : \Delta \mathbf{e}, \\ \boldsymbol{\tau}_{pr} &= \boldsymbol{\sigma}_{pr} \cdot \mathbf{n}, & \Delta \boldsymbol{\tau}^{tr} &= \Delta \boldsymbol{\sigma}^{tr} \cdot \mathbf{n}, \\ \mathbf{m}^* &= \frac{\mathbf{A}_d \cdot \boldsymbol{\tau}}{\bar{\tau}_0 \tau^{e*}}, & \mathbf{m}^e &= \bar{u}_0 \mathbf{m}^*, \\ \mathbf{M}^* &= \frac{1}{2}(\mathbf{n} \otimes \mathbf{m}^* + \mathbf{m}^* \otimes \mathbf{n}), & \mathbf{M}^e &= \frac{\bar{u}_0}{L_e} \mathbf{M}^*, \\ \boldsymbol{\sigma}_m &= \mathbf{E} : \mathbf{M}^e, & \boldsymbol{\tau}_m &= \boldsymbol{\sigma}_m \cdot \mathbf{n}, \\ \Delta \mathbf{e}^d &= \Delta \lambda \mathbf{M}^e, & \Delta \mathbf{u}^p &= \Delta \lambda \mathbf{m}^e, \\ \Delta \boldsymbol{\tau} &= \Delta \boldsymbol{\tau}^{tr} - \Delta \lambda \boldsymbol{\tau}_m, & \boldsymbol{\tau} &= \boldsymbol{\tau}_{pr} + \Delta \boldsymbol{\tau}, \\ \mathbf{u}^p &= \mathbf{u}_{pr}^p + \Delta \mathbf{u}^p, & \lambda &= \lambda_{pr} + \Delta \lambda, \\ \bar{\tau}^* &= \lambda^q, & \tau^{e*} &= \frac{1}{\bar{\tau}_0} (\boldsymbol{\tau} \cdot \mathbf{A}_d \cdot \boldsymbol{\tau})^{1/2}, \\ F_d^* &= \tau^{e*} - (1 - \bar{\tau}^*) = 0, \\ \boldsymbol{\sigma} &= \boldsymbol{\sigma}^{tr} - \Delta \lambda \boldsymbol{\sigma}_m. \end{aligned} \quad (42)$$

The first step is to assume that no decohesion occurs, to obtain a trial stress and traction:

$$\boldsymbol{\sigma}^{tr} = \boldsymbol{\sigma}_{pr} + \Delta \boldsymbol{\sigma}^{tr}, \quad \boldsymbol{\tau}^{tr} = \boldsymbol{\sigma}^{tr} \cdot \mathbf{n} \quad (43)$$

and then determine the value of the damage function, F_d^{*tr} , for this trial traction and the existing value λ_{pr} . If $F_d^{*tr} \leq \varepsilon$ where ε is a user-prescribed tolerance, then the step is purely elastic with no additional decohesion and no further action is required. If the inequality is not satisfied, the decohesion variables must be incremented.

Next we describe a one-step algorithm which enforces the requirement $F_d = 0$ to order $(\Delta\lambda)^3$. Perform a Taylor expansion of F_d about the trial state:

$$F_d = a(\Delta\lambda)^2 + 2b\Delta\lambda + c + O(\Delta\lambda)^3 \tag{44}$$

in which the last term indicates the order of the remainder and

$$a = \frac{1}{2} \frac{\partial^2 F_d}{\partial \lambda^2} \Big|_{tr}, \quad 2b = \frac{\partial F_d}{\partial \lambda} \Big|_{tr}, \quad c = F_d^{tr}. \tag{45}$$

We choose $\Delta\lambda = \Delta\lambda_1$ and $\Delta\lambda = \Delta\lambda_2$ to be the solutions to the first-order and second-order equations, respectively; i.e., $2b\Delta\lambda_1 + c = 0$ and $a(\Delta\lambda_2)^2 + 2b\Delta\lambda_2 + c = 0$ or

$$\Delta\lambda_1 = -\frac{c}{2b}, \quad \Delta\lambda_2 = \frac{-b + \sqrt{b^2 - ac}}{a} \tag{46}$$

with the sign chosen so that in the limit of infinitesimal $\Delta\lambda$ we have $\Delta\lambda_2 = \Delta\lambda_1$.

Consider the case when the model choice of (19) is used and the Taylor expansion is applied to the dimensionless damage function F_d^* . It follows from (45) that

$$\begin{aligned} c &= (\tau^{e^*})^{tr} - (1 - \lambda_{pr}^q) \\ 2b &= \frac{\partial \tau^{e^*}}{\partial \tau} \cdot \frac{\partial \tau}{\partial \lambda} + q\lambda_{pr}^{q-1} \\ 2a &= \frac{\partial \tau}{\partial \lambda} \cdot \frac{\partial^2 \tau^{e^*}}{\partial \tau^2} \cdot \frac{\partial \tau}{\partial \lambda} + \frac{\partial \tau^{e^*}}{\partial \tau} \cdot \frac{\partial^2 \tau}{\partial \lambda^2} + q(q-1)\lambda_{pr}^{q-2} \end{aligned} \tag{47}$$

in which all terms are to be evaluated at λ_{pr} and the trial value of the traction. Note that when $q = 1$, the last term in the expression for a is zero. With a modest amount of algebra involving (42), it follows that

$$\frac{\partial \tau}{\partial \lambda} = -\tau_m, \quad \frac{\partial \tau^{e^*}}{\partial \tau} = \frac{\mathbf{m}^*}{\bar{\tau}_0} \tag{48}$$

and we immediately have the relation

$$2b = -\frac{\mathbf{m}^* \cdot \tau_m}{\bar{\tau}_0} + q\lambda_{pr}^{q-1}. \tag{49}$$

Next, we proceed to obtain the coefficient a in (47). We utilize (42) and (48) to obtain

$$\frac{\partial^2 \tau^{e^*}}{\partial \tau^2} = \frac{1}{\bar{\tau}_0^2 \tau^{e^*}} [\mathbf{A}_d - \mathbf{m}^* \otimes \mathbf{m}^*] \tag{50}$$

which leads to

$$\frac{\partial \tau}{\partial \lambda} \cdot \frac{\partial^2 \tau^{e^*}}{\partial \tau^2} \cdot \frac{\partial \tau}{\partial \lambda} = \frac{[(\tau_m \cdot \mathbf{A}_d \cdot \tau_m) - (\tau_m \cdot \mathbf{m}^*)^2]}{\bar{\tau}_0^2 \tau^{e^*}}. \tag{51}$$

Finally

$$\frac{\partial^2 \tau}{\partial \lambda^2} = -\frac{\partial \tau_m}{\partial \lambda} = -\mathbf{n} \cdot \mathbf{E} : \frac{\partial \mathbf{M}^*}{\partial \lambda} = -\mathbf{n} \cdot \mathbf{E} : \frac{\bar{\mathbf{u}}_0}{L_c} \left(\mathbf{n} \otimes \frac{\partial \mathbf{m}^*}{\partial \lambda} \right) \tag{52}$$

in which the minor symmetry of \mathbf{E} has been used. We note that

$$\begin{aligned} \frac{\partial \mathbf{m}^*}{\partial \lambda} &= \frac{\partial \mathbf{m}^*}{\partial \boldsymbol{\tau}} \cdot \frac{\partial \boldsymbol{\tau}}{\partial \lambda} = -\frac{1}{\bar{\tau}_0} \frac{\partial^2 \tau^{e^*}}{\partial \boldsymbol{\tau}^2} \cdot \boldsymbol{\tau}_m = -\frac{1}{\bar{\tau}_0} [\mathbf{A}_d - \mathbf{m}^* \otimes \mathbf{m}^*] \cdot \boldsymbol{\tau}_m \\ \frac{\partial \tau^{e^*}}{\partial \boldsymbol{\tau}} \cdot \left(-\mathbf{n} \cdot \mathbf{E} \cdot \frac{\bar{\mathbf{u}}_0}{L_c} \mathbf{n} \right) &= -\frac{1}{\bar{\tau}_0} (\mathbf{m}^* \otimes \mathbf{n}) : \mathbf{E} \cdot \frac{\bar{\mathbf{u}}_0}{L_c} \mathbf{n} = -\frac{\boldsymbol{\tau}_m}{\bar{\tau}_0} \end{aligned} \tag{53}$$

with the result

$$\frac{\partial \tau^{e^*}}{\partial \boldsymbol{\tau}} \cdot \frac{\partial^2 \boldsymbol{\tau}}{\partial \lambda^2} = \frac{[(\boldsymbol{\tau}_m \cdot \mathbf{A}_d \cdot \boldsymbol{\tau}_m) - (\boldsymbol{\tau}_m \cdot \mathbf{m}^*)^2]}{\bar{\tau}_0^2 \tau^{e^*}}, \tag{54}$$

a result identical to that of (51). Therefore

$$a = \frac{[(\boldsymbol{\tau}_m \cdot \mathbf{A}_d \cdot \boldsymbol{\tau}_m) - (\boldsymbol{\tau}_m \cdot \mathbf{m}^*)^2]}{\bar{\tau}_0^2 \tau^{e^*}} + \frac{q(q-1)}{2} \lambda_{pr}^{q-2}. \tag{55}$$

Even with this rather simple form, preliminary numerical results indicate that the use of the first-order equation for $\Delta \lambda_1$ in (46) is sufficiently accurate and the extra computations required to obtain the parameter given by (55) is not justified.

4.3. Separation

The procedure outlined above holds until either one of two situations arises. The first is that of traction reversal at the element level and the second is that of separation. The solution algorithm is predicated on a prescribed strain increment that would have to be released for traction reversal. The manifestation of such a possibility is that a solution does not exist for the discrete constitutive equation. Near separation, a solution also may not exist but now the reason is that numerical overflow or underflow may occur because both the numerator and denominator are close to zero in the determination of \mathbf{m}^* . Therefore, an alternative procedure described next must be implemented for the state of separation. The algorithm can also be considered one for enforcing a stress-free boundary condition through the decohesive constitutive equation subroutine.

Consider local coordinates, $n-t$, associated with the failure surface and suppose the trial stress has been obtained. The updated components of the stress are given in vector form as follows:

$$\begin{Bmatrix} \sigma_{nn} \\ \sigma_{tt} \\ \sigma_{nt} \end{Bmatrix} = \begin{Bmatrix} \sigma_{nn}^{tr} \\ \sigma_{tt}^{tr} \\ \sigma_{nt}^{tr} \end{Bmatrix} - \begin{bmatrix} E_1 & E_2 & 0 \\ E_2 & E_1 & 0 \\ 0 & 0 & 2G \end{bmatrix} \begin{Bmatrix} \Delta e_{nn}^d \\ \Delta e_{tt}^d \\ \Delta e_{nt}^d \end{Bmatrix} \tag{56}$$

where E_1 and E_2 are components of the isotropic elasticity matrix for the planar situation under consideration. Solutions for σ_{tt} , Δe_{nn}^d and Δe_{nt}^d subject to the constraints that $\sigma_{nn} = 0$, $\sigma_{nt} = 0$ and $\Delta e_{nt}^d = 0$ are given as follows:

$$\begin{aligned} \Delta e_{nt}^d &= \frac{\sigma_{nt}^{tr}}{2G}, \\ \Delta e_{nn}^d &= \frac{\sigma_{nn}^{tr}}{E_1}, \\ \sigma_{tt} &= \sigma_{tt}^{tr} - E_2 \Delta e_{nn}^d. \end{aligned} \tag{57}$$

Next, (39)–(41) are used to relate the increments in decohesion strain to the magnitude of the displacement discontinuity, Δu^d , and the components of the displacement discontinuity, $\Delta \mathbf{u}^d = \Delta u^d \mathbf{m}$ with the result

$$\Delta u_n^d = L_c \Delta e_{nn}^d, \quad \Delta u_t^d = L_c \Delta e_{nt}^d. \tag{58}$$

Finally, the increments in the magnitude of the discontinuity, Δu^d , and decohesion parameter, $\Delta\lambda = \Delta u^d / \bar{u}_0$, are obtained.

The separation algorithm is invoked when either traction reversal is sensed (no solution to the standard decohesion algorithm) or separation is imminent ($\lambda > 0.98$, say). For the problems considered, no significant difference in solution is observed if one merely invokes the separation algorithm for $\lambda > 0.8$.

4.4. Example solutions

The applications given in this section are restricted to cases made with the following assumptions:

- (i) The initiation of failure is given directly by a failure criterion rather than by a discontinuous bifurcation analysis, and
- (ii) The problems are limited to those for which the orientations of the surfaces of decohesion are known, a priori. Delamination constitutes one member of this class of problems.

The objectives of performing these numerical analyses are the following:

- (i) To illustrate that the use of jump in displacement as an internal variable together with a weak implementation of compatibility provides a simple and useful algorithm in the MPM.
- (ii) To show that the MPM does not exhibit the finite element pathologies associated with distorted meshes and instabilities with the result that additional features such as enhanced strains are not required.
- (iii) To illustrate by example that the material point method does not exhibit the orientation effect often seen with finite elements when discontinuities are allowed to propagate at various angles to the mesh sides.

As described by Allix et al. [1], delamination can be a complex process of degradation of both the layers and the bonds between the layers. Here, we do not attempt to follow all details of the microstructural process but attempt to represent the most important aspects with the simplified version of decohesion involving plasticity, values of traction at which decohesion is initiated, and invariance of energy dissipation with mesh refinement.

The computational domain for the model problem is illustrated in Fig. 5 for an axially loaded bar with a height to length ratio of 1:6. The right end of the bar is fixed and the other end is loaded through the artifice of a rigid head with large mass moving at a uniform, constant speed 0.001 to the left. The inclination of the laminates is identified by the angle α with respect to the x -axis as defined in Fig. 2. Solutions are obtained by explicit time integration applied to the dynamic equations with a mass density of 1. A quasistatic solution is obtained by ensuring that the duration of loading is several times the elastic wave transit time for the bar.

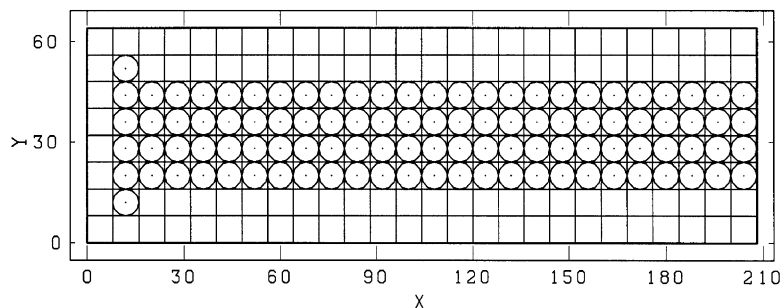


Fig. 5. Computational domain for model problem.

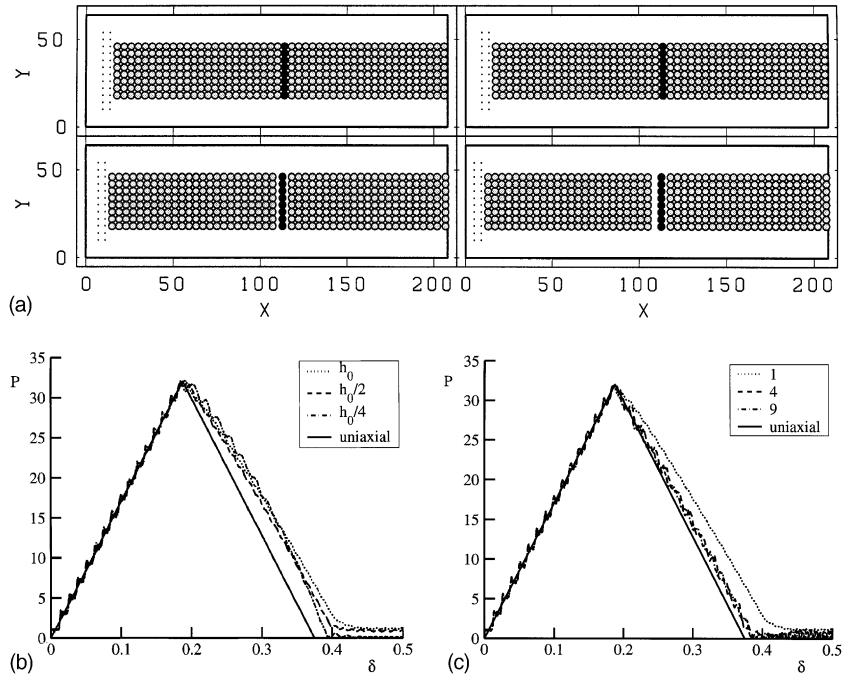


Fig. 6. Propagation of delamination through the grid for transverse laminates: (a) plots of material points for end displacements of 0.25, 0.50, 3.0 and 5.0, (b) load–displacement curves for various degrees of mesh refinement, (c) load–displacement curves for various numbers of material points per element.

All geometric and material parameters are dimensionless. For convenient display of numerical data, especially with regard to the convergence study, the height and length of the bar are chosen to be $H = 32$ and $L = 192$, respectively. Square elements are used for all cases. The coarsest mesh consists of elements with size $h_0 = 8$, a time step of $\Delta t = 0.1$ and one material point per element as shown in Fig. 5. The computational domain provides two rows of elements on each side of the bar when $h = 8$. Mesh refinement studies consist of cutting h and Δt by a factor of 2 for each refinement. For the numerical simulations, an imperfection in the form of a 10% reduction in τ_{nf} at one point is used to control the location of the failure surface.

The material is elastic with Young's modulus chosen to be 1024 and Poisson's ratio is 0.25. The decohesion formulation is invoked with evolution functions based on an associated rule for all cases.

The first set of numerical results shown in Fig. 6 is based on traction-failure values of $\tau_{nf} = 1$ and $\tau_{nf} = 10$ to simulate a discontinuity that is primarily in the normal direction (Mode I) for a laminate angle of $\alpha = 90^\circ$. The reference surface energy is chosen to be $U_0 = \bar{u}_0$ so that the reference traction is $\bar{\tau}_0 = 1$ since $U_0 = \bar{u}_0 \bar{\tau}_0$. The first equation of (30) yields $\sigma_0 = 1$. The effective decohesion at failure is chosen to be $\bar{u}_0 = L/512 = 0.375$ so that (36) yields $\eta = 2$ for $\alpha = 90^\circ$. Snap back is precluded because $\eta > 1$. The initial imperfection was placed at the center of the bar. For the medium mesh consisting of elements with each side $h = h_0/2 = 4$, the effective decohesion \bar{u} (which for this case is approximately the normal component, u_n^p) is indicated in gray scale in Fig. 6(a) with the lightest value being zero. The primary point to emphasize here is that the decohesive zone does not become diffuse as it propagates across the mesh. In fact it appears that all of the discontinuity is identified with a single line of elements. Furthermore, complete separation is modeled by doing nothing more than maintaining zero traction on the failure surface through the decohesive constitutive equation. Each material point that exhibits the discontinuity can be located anywhere spatially

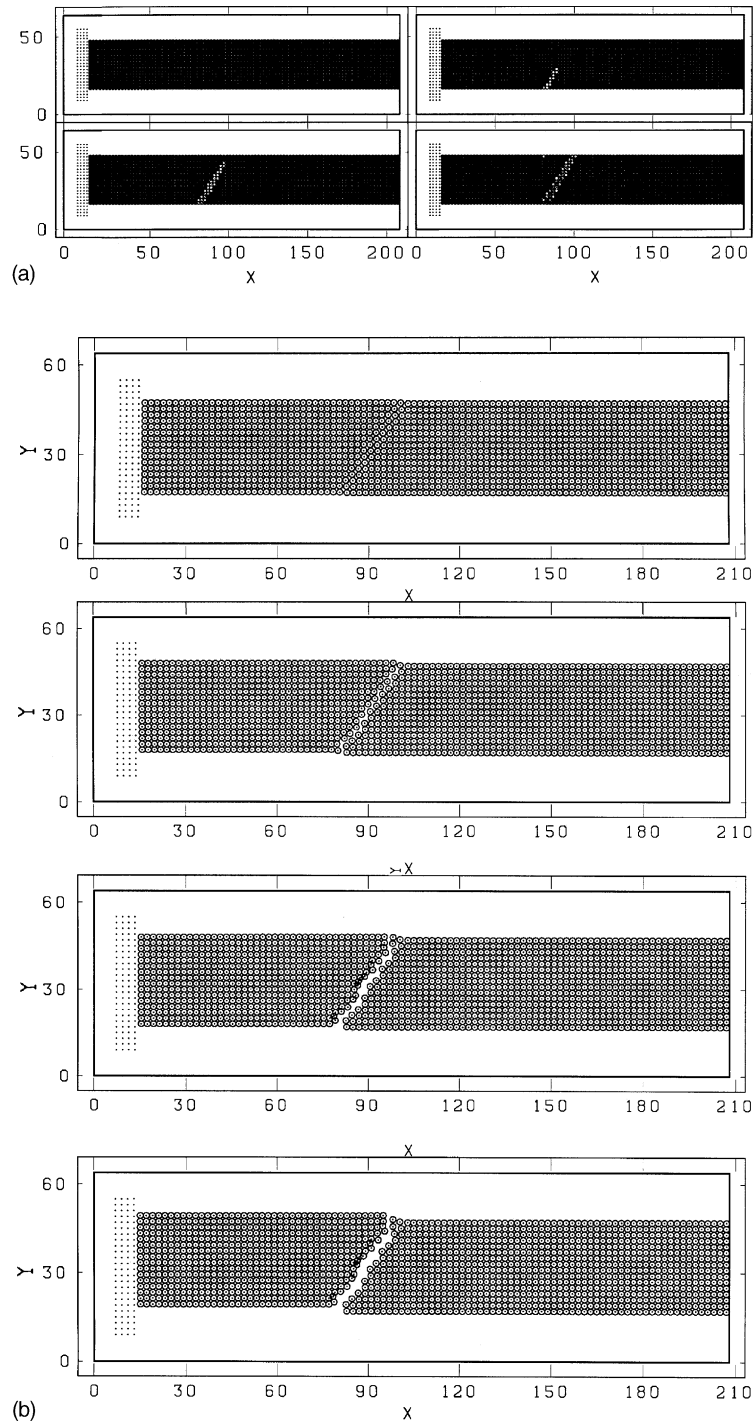


Fig. 7. Propagation of Mode I delamination through the grid for laminates at an angle of $\alpha = 60^\circ$: (a) contour plots of decohesion for end deflections of 0.24, 0.25, 0.26 and 0.28, (b) plots of material points for end displacements of 0.7, 1.2, 1.7 and 2.0, (c) displacement trajectories for an end displacement of 0.35, (d) load–deflection plot.

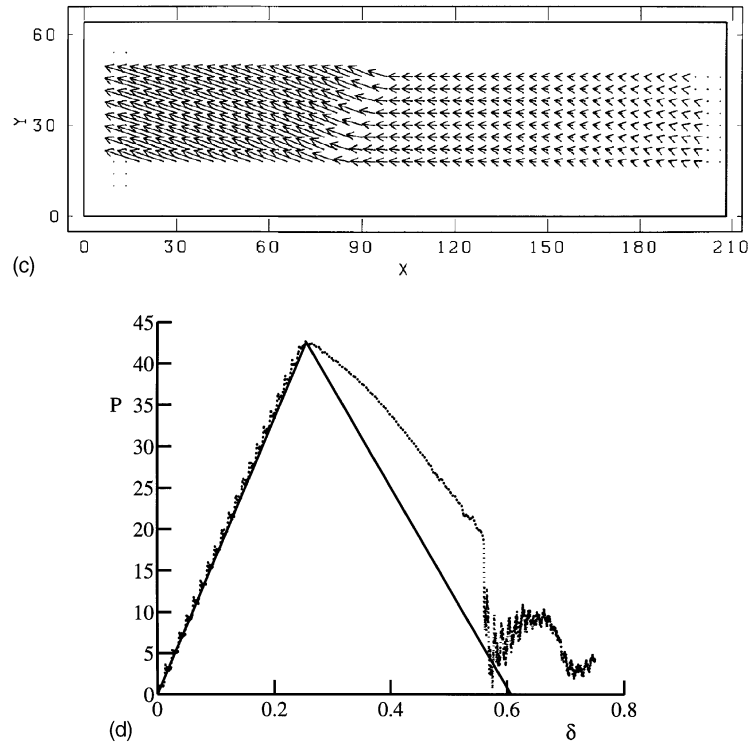


Fig. 7 (continued)

between the adjacent material points associated with material that has not failed. This feature is merely a manifestation of associating a discontinuity with a material point with the implication that one material point is identified with an infinite number of spatial points (Fig. 1). The frames in Fig. 6(a) correspond to end deflections of 0.25, 0.50, 3.0 and 5.0, respectively.

The peak load on the bar is simply the product of the failure traction, $\tau_{nf} = 1$, times the width of the bar, $H = 32$. With the problem parameters specified above, the slope of the load–deflection curve in the elastic regime is $dP/d\delta = 171$. Similarly, the use of (37) with $\eta = 2$ yields $dP/d\delta = -171$ when the material is failing. These results are plotted as the uniaxial solution in Fig. 6(b) together with numerical results for various degrees of mesh refinement. The numerical results are essentially equivalent but with a slight discrepancy from the exact solution because the numerical approach with one material point per element simulates a propagating crack that may cause a slight variation from uniaxial stress whereas the exact solution is based on the premise that the crack opening is the same everywhere across the bar. There is a slight improvement with mesh refinement for one material point per element in the prediction of the total deflection at separation. However, as shown in Fig. 6(c) for a course mesh, the agreement between the numerical and uniaxial solutions is considerably better when four material points per element are used. The use of nine material points per element produces no significant improvement over four material points.

Next, the results of numerical calculations are given in Fig. 7 for delamination at an angle of $\alpha = 60^\circ$ for the case of a Mode I simulation obtained by utilizing the same decohesion parameters as those used for the previous problem. The use of (30) and (36) yields $\eta = 1.3$ so the uniaxial stress solution again indicates no snapback. First, the predicted propagation is shown as contour plots in Fig. 7(a) for the fine mesh of $h = 2$ and for the relatively small values of end deflections of 0.24, 0.25, 0.26 and 0.28, respectively. This result shows that the propagation direction through the mesh is very close to the angle specified in the constitutive

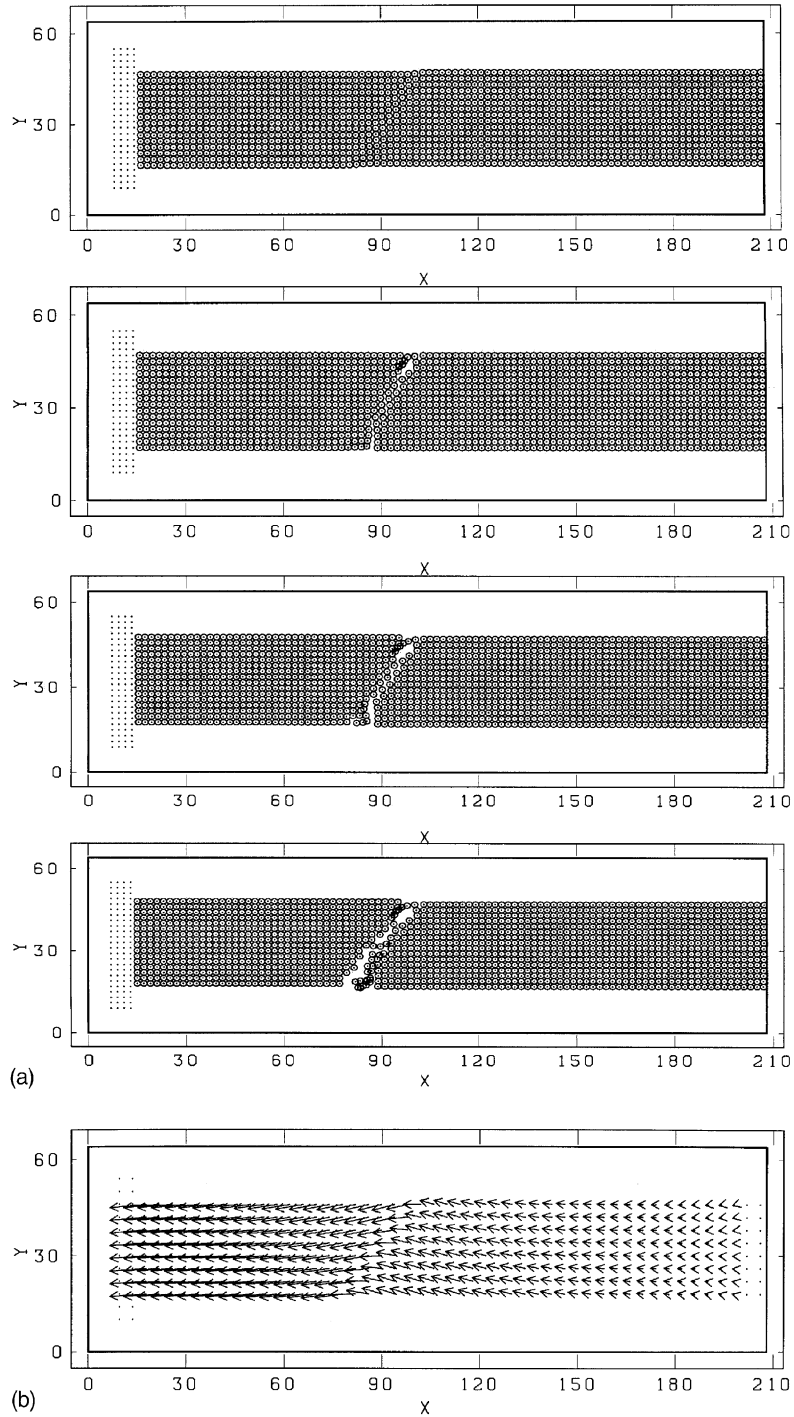


Fig. 8. Propagation of Mode II delamination through the grid for laminates at an angle of $\alpha = 60^\circ$: (a) plots of material points for end displacements of 0.7, 1.2, 1.7 and 2.0, (b) displacement trajectories for an end displacement of 0.35, (c) load–deflection plot.

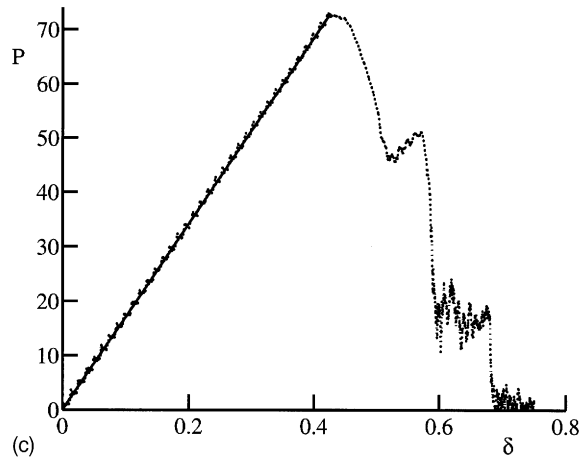


Fig. 8 (continued)

equation. This is an important feature because there is no special algorithm to enforce compatibility in a manner analogous to remeshing that, for example, is often used in the finite element literature to align element sides with an evolving crack. However, predictions of decohesion now occur in a zone with a bandwidth encompassing approximately two elements.

In Fig. 7(b), we show plots of material points at the relatively large end deflections of 0.7, 1.2, 1.7 and 2.0, respectively. These plots are given to show that separation is clearly indicated and that this feature is also obtained without the need for remeshing or special kinematic feature other than enforcing the traction-free condition through the constitutive equation subroutine. The displacement trajectories at an end displacement of 0.35 are shown in Fig. 7(c). Load–deflection plots are shown in Fig. 7(d) together with the analytical solution based on the assumption of uniaxial stress. As seen, there is some discrepancy which can be attributed to two sources: (i) the initiation and propagation of the crack is associated with a localized field that is not uniaxial stress in the interior of the bar, and (ii) decohesion is predicted for material points located in a zone that is approximately two elements wide. The latter situation exists because there is no kinematic construction in the displacement field to accommodate a crack across elements. The net effect is that the dispersed failure zone causes more energy to be dissipated than a single failure plane with the consequence that the softening slope of the load–deflection curve is less than the exact slope. To compensate for the excess dissipation one might reduce the softening parameter in the decohesive constitutive equation to achieve the correct global dissipation based on the fracture energy for the material and the area of the fracture zone. Finally, because of the small slope in the softening portion of the load–displacement curve relative to the exact solution for uniaxial stress, the condition for a load reversal is met for the numerical solution. Rather than implementing a procedure to handle the load reversal as indicated by a lack of solution for the constitutive equation subroutine, the traction is merely dropped to zero. This accounts for the abrupt drop in the force and the subsequent ringing.

Finally, a simulation of Mode II failure with $\alpha = 60^\circ$ was performed through the artifice of setting $\tau_{nf} = 10$ and $\tau_{tf} = 1$. The other parameters were chosen to be $\bar{\tau}_0 = \tau_{nf}$ and $U_0 = 0.375$. For this mode of failure and these parameters, the uniaxial analysis indicates that load reversal should occur ($\eta = 0.43$). However, because of the dispersed failure zone, load reversal is not detected numerically. This provides another indication that a larger softening modulus should be specified when cracking at angles other than 0° or 90° is observed. The locations of material points at the relatively large end deflections of 0.7, 1.2, 1.7 and 2.0, respectively, are given in Fig. 8(a). The first (top) plot shows the end of the decohesion process in

Mode II and the subsequent plots are showing locations of material points as separation occurs. The separation is not as clean as that shown for Mode I in Fig. 7(b) as indicated by the upward displacement of the left side of the bar after separation. A close examination of the stress field shows that just prior to separation significant axial stresses are built up in the region adjacent to the lower and upper boundaries. These stresses are of opposite sign so an internal moment is being developed as is a resultant shear along a vertical plane at the midsection of the bar. It is this vertical shear force that imparts a vertical velocity to the left (unconstrained) portion of the bar with the consequence that the left portion shows a displacement after decohesion. The source of the axial stresses and the transverse shear could be due to the fact that the algorithm imparts a single-valued velocity field to all material points within an element and until the separation is at least one cell wide, such relatively small perturbations to the stress field may be present. These modifications to the stress field may also be causing the variations to the expected smooth and monotonically decaying feature of the load–displacement plot shown in Fig. 8(c).

Similar analyses have been performed for laminate angles of $\alpha = 45^\circ$ and $\alpha = 30^\circ$ [45].

5. Summary

A rigid, plastically softening decohesion model has been combined with continuum elasticity and traction continuity at a material failure surface to provide a relatively simple description for the evolution of material failure. When incorporated in the material point method, the result is a constitutive equation subroutine that is similar to softening plasticity. A length parameter associated with a material element provides a mechanism for ensuring convergence with mesh refinement. As the tip of a failure surface propagates through the mesh, the formulation inherent with the material point method appears to preclude the diffusion of the crack tip, a feature often seen with conventional finite elements. Further investigations involving the propagation of curved cracks is necessary to determine whether or not the proposed method is general and robust. Nevertheless, in light of the long history of complex numerical analyses in connection with crack propagation, we believe the simplicity of the decohesion formulation in the material point method holds considerable promise for development into a general method for predicting the evolution of material failure.

Acknowledgements

This work was partially supported by Los Alamos National Laboratory, Sandia National Laboratories, the Air Force Office of Scientific Research and the National Science Foundation. The first author greatly appreciates the support of Professor G. Baker and the Civil Engineering Department the University of Queensland, Australia to work on this problem while on sabbatical leave from the University of New Mexico.

References

- [1] O. Allix, P. Ladavéze, A. Corigliano, Damage analysis of interlaminar fracture specimens, *Compos. Struct.* 31 (1995) 61–74.
- [2] O. Allix, A. Corigliano, Modeling and simulation of crack propagation in mixed-modes interlaminar fracture specimens, *Int. J. Fract.* 77 (1996) 111–140.
- [3] F. Armero, K. Garikipati, An analysis of strong discontinuities in multiplicative finite strain plasticity and their relation with the numerical simulation of strain localization in solids, *Int. J. Solid Struct.* 33 (1996) 2863–2885.
- [4] F. Armero, Large-scale modeling of localized dissipative mechanisms in a local continuum: applications to the numerical simulation of strain localization in rate-dependent inelastic solids, *Mech. Cohes-Frict. Mater.* 4 (1999) 101–131.

- [5] Z.P. Bazant, B.H. Oh, Crack band theory for fracture of concrete, *Mater. Struct. RILEM* 16 (1983) 155–177.
- [6] G.I. Barenblatt, The formation of equilibrium cracks during brittle fracture; general ideas and hypotheses: axially symmetric cracks, *J. Appl. Math. Mech.* 23 (1959) 622–636.
- [7] T. Belytschko, Y. Krongauz, D. Organ, M. Fleming, P. Krysl, Meshless methods: an overview and recent developments, *Comput. Meth. Appl. Mech. Engrg.* 139 (1–4) (1996) 3–48.
- [8] G.T. Camacho, M. Ortiz, Computational modelling of impact damage in brittle materials, *Int. J. Solid Struct.* 33 (20–22) (1996) 2899–2938.
- [9] A. Corigliano, Formulation, identification and use of interface models in the numerical analysis of composite delamination, *Int. J. Solid Struct.* 30 (20) (1993) 2779–2811.
- [10] O. Dahlbom, N.S. Ottosen, Smearred crack analysis using generalized fictitious crack model, *J. Engrg. Mech.* 116 (1990) 55–76.
- [11] R. de Borst, Smearred cracking plasticity creep and thermal loading—a unified approach, *Comput. Meth. Appl. Mech. Engrg.* 72 (1987) 89–110.
- [12] E. Dvorkin, A.M. Cuitiño, Gioai, Finite elements with displacement interpolated embedded localization lines insensitive to mesh size and distortions, *Int. J. Numer. Meth. Engrg.* 30 (1990) 541–564.
- [13] P.H. Feenstra, R. de Borst, J.G. Rots, Numerical study of crack dilatancy. I: models and stability analysis, *J. Engrg. Mech.* 117 (1991a) 733–753.
- [14] P.H. Feenstra, R. de Borst, J.G. Rots, Numerical study of crack dilatancy. II: applications, *J. Engrg. Mech.* 117 (1991b) 754–769.
- [15] A. Hillerborg, M. Modéer, P.-E. Petersson, Analysis of crack formation and crack growth in concrete by means of fracture mechanics and finite elements, *Cem. Concr. Res.* 6 (1976) 773–782.
- [16] A.D. Jefferson, Plastic-damage model for interfaces in cementitious materials, *J. Engrg. Mech.* 124 (1998) 775–782.
- [17] G.R. Johnson, R.A. Stryk, S.R. Beissel, SPH for high velocity impact computations, *Comput. Meth. Appl. Mech. Engrg.* 139 (1–4) (1996) 347–374.
- [18] M. Klisinski, K. Runesson, S. Sture, Finite element with inner softening band, *J. Engrg. Mech.* 117 (1991) 575–587.
- [19] R. Larsson, K. Runesson, Element-embedded localization band based on regularized displacement discontinuity, *J. Engrg. Mech.* 122 (5) (1996) 402–411.
- [20] W.K. Liu, Y. Chen, R.A. Uras, C.T. Chang, Generalized multiple scale reproducing kernel particle methods, *Comput. Meth. Appl. Mech. Engrg.* 139 (1–4) (1996) 91–158.
- [21] J.M. Melenk, I. Babushka, The partition of unity finite element method: basic theory and applications, *Comput. Meth. Appl. Mech. Engrg.* 139 (1–4) (1996) 289–314.
- [22] A. Needleman, A continuum model for void nucleation by inclusion debonding, *J. Appl. Mech.* 54 (1987) 525–531.
- [23] J. Oliver, A consistent characteristic length for smearred cracking problems, *Int. J. Numer. Meth. Engrg.* 28 (1989) 461–474.
- [24] J. Oliver, Modelling strong discontinuities in solid mechanics via strain softening constitutive equations. Part 1: fundamentals, *Int. J. Numer. Meth. Engrg.* 39 (1996) 3575–3600.
- [25] J. Oliver, Modelling strong discontinuities in solid mechanics via strain softening constitutive equations. Part 2: numerical simulations, *Int. J. Numer. Meth. Engrg.* 39 (1996) 3601–3623.
- [26] J. Oliver, On the discrete constitutive models induced by strong discontinuity kinematics and continuum constitutive equations, *Int. J. Solid Struct.* 37 (48–50) (2000) 7207–7230.
- [27] M. Ortiz, A. Pandolfi, A class of cohesive elements for the simulation of three-dimensional crack propagation, *Int. J. Numer. Meth. Engrg.* 44 (1999) 1267–1282.
- [28] J. Planas, M. Elices, G.V. Guinea, The extended cohesive crack, in: G. Baker, B.L. Karihaloo (Eds.), *Fracture of Brittle Disordered Materials: Concrete, Rock and Ceramics*, E&FN Spon, London, 1995, pp. 51–65.
- [29] A. Pandolfi, P.R. Guduru, M. Ortiz, A.J. Rosakis, Three dimensional cohesive-element analysis and experiments of dynamic fracture in C300 steel, *Int. J. Solid Struct.* 37 (2000) 3733–3760.
- [30] P.W. Randles, L.D. Libersky, Smoothed particle hydrodynamics: some recent improvements and applications, *Comput. Meth. Appl. Mech. Engrg.* 139 (1–4) (1996) 375–408.
- [31] E.D. Reedy Jr., F.J. Mello, T.R. Guess, Modelling the initiation and growth of delaminations in composite structures, *J. Compos. Struct.* 31 (1997) 812–831.
- [32] J.G. Rots, R. de Borst, Analysis of mixed-mode fracture in concrete, *J. Engrg. Mech.* 113 (1987) 1739–1758.
- [33] J.C.J. Schellekens, Computational strategies for composite structures, Ph.D. Dissertation, Department of Civil Engineering, The Delft University of Technology, Delft, The Netherlands, 1992.
- [34] J.C. Simo, J. Oliver, F. Armero, An analysis of strong discontinuities induced by strain-softening in rate-independent solids, *Comput. Mech.* 12 (1993) 277–296.
- [35] J.C. Simo, J. Oliver, A new approach to the analysis and simulation of strain-softening in solids, in: Z.P. Bazant et al. (Eds.), *Fracture and Damage in Quasi-Brittle Materials*, Workshop held in Prague, 1994.
- [36] Z. Suo, M. Ortiz, A. Needleman, Stability of solids with interfaces, *J. Mech. Phys. Solid* 40 (1) (1992) 613–640.
- [37] D. Sulsky, Z. Chen, H.L. Schreyer, A particle method for history-dependent materials, *Comput. Meth. Appl. Mech. Engrg.* 118 (1994) 179–196.

- [38] D. Sulsky, S.-J. Zhou, H.L. Schreyer, Application of a particle-in-cell method to solid mechanics, *Comput. Phys. Commun.* 87 (1&2) (1995) 236–252.
- [39] D. Sulsky, H.L. Schreyer, Axisymmetric form of the material point method with applications to upsetting and Taylor impact problems, *Comput. Meth. Appl. Mech. Engrg.* 139 (1–4) (1996) 409–429.
- [40] K. Szuwalski, M. Zyczkowski, On the Phenomenon of decohesion in perfect plasticity, *Int. J. Solid Struct.* 9 (1973) 85–98.
- [41] G.N. Wells, L.J. Sluys, Application of embedded discontinuities for softening solids, *Engrg. Fract. Mech.* 65 (2000) 263–281.
- [42] G.N. Wells, L.J. Sluys, Three-dimensional embedded discontinuity model for brittle fracture, *Int. J. Solid Struct.* 38 (5) (2001) 897–913.
- [43] G.N. Wells, L.J. Sluys, Discontinuous analysis of softening solids under impact loading, *Numer. Anal. Meth. Geomech.* 25 (7) (2001) 691–709.
- [44] S. Wiehe, B. Kroplin, R. de Borst, Classification of smeared crack models based on material and structural properties, *Int. J. Solid Struct.* 35 (12) (1998) 1289–1312.
- [45] S. Zhou, The numerical prediction of material failure based on the material point method, Ph.D. Dissertation, Department of Mechanical Engineering, The University of New Mexico, Albuquerque, NM, 1998.